A R C H I V E S O F M E T A L L U R G Y A N D M A T E R I A L S
Volume 50 2005 Issue 2

Z. ŚWIĄTEK*, A. BONCHYK**, I.M. FODCHUK*** I.V. LITVINCHUK***, W. BALIGA*, M. MICHALEC****, J. GUŚPIEL*

COMPLEX PHOTOLUMINESCENCE SPECTRUM OF Si NANOSTRUCTURES FORMED BY THE ION IMPLANTATION AND CHEMICAL ETCHING

ZŁOŻONE WIDMO FOTOLUMINESCENCJI NANOSTRUCTUR KRZEMOWYCH WYTWORZONYCH POPRZEZ IMPLANTACJĘ JONOWĄ I TRAWIENIE CHEMICZNE

Photoluminescence spectroscopy, AFM and non-destructive X-ray diffraction methods were used to study photoluminescence mechanism in silicon nanostructure formed by chemical etching on the n^+-type, (111)- oriented Si wafer with buried heavily damaged (BHD) thin layer. The BHG layer was produced by the phosphorous ion implantation followed by thermal treatment in nitrogen atmosphere. The final nanostructures were formed (on a half of the implanted and non-implanted areas only) by electroless chemical etching. Implanted and non-implanted areas of the Si wafer were used as standards to observe changes in near-surface layers of silicon crystal during the nanostructure formation.

We show that the porous silicon thin film produced by the ion implantation and chemical etching exhibits a room temperature photoluminescence at 400 — 700nm, while the thin porous silicon layer obtained on unimplanted substrate at ~550 - 750nm.

The model of structural changes in the near-surface layers of the Si wafer after applied technological processes as well as the mechanisms of the elementary bands in photoluminescence spectra are proposed..

W badaniach mechanizmu fotoluminescencji nanostruktury krzemowej wytworzonej w procesie trawienia chemicznego płytki krzemowej typu n^+ o orientacji (111) i posiadającej silnie zdefektowaną warstwę „zagrzebaną", wykorzystano spektroskopię fotoluminescencji, mikroskop sił atomowych oraz nieniszczące metody dyfrakcji rentgenowskiej.

Zagrzebaną warstwę zdefektowaną wytworzono w procesie implantacji jonów fosforu i obróbki termicznej. Podczas implantacji jonowej połowa płytki krzemowej była ekranowana. Ostateczne nanostruktury uzyskano (jedynie na połowie obszaru implantowanego i nieimplantowanego) w procesie trawienia chemicznego. W obserwacjach zmian strukturalnych

* INSTYTUT METALURGII I INŻYNIERII MATERIAŁOWEJ IM. A. KRUPKOWSKIEGO, POLSKA AKADEMIA NAUK, 30-059 KRAKÓW, UL. REYMONTA 25

** INSTITUTE FOR APLIED PROBLEMS OF MECHANICS AND MATHEMATICS OF NASU, 3-B NAUKOVA STR., 79601 LVLV UKRAINE

*** CHERNIVTSI STATE UNIVERSITY, 274012 CHERNIVTSI, 2 KOTSYUBYNSKY STR., UKRAINE

**** WYDZIAŁ CHEMII, UNIWERSYTET JAGIELLOŃSKI, 30-069 KRAKÓW, UL. INGARDENA 3

w obszarach przypowierzchniowych kryształu krzemu zachodzących podczas formowania nanostruktury, obszary implantowany i nieimplantowany posłużyły jako wzorce. Nanokrystaliczna cienka warstwa krzemu otrzymana na drodze implantacji jonowej i trawienia chemicznego wykazuje fotoluminescencję w zakresie długości fali od 400 do 700μm, podczas gdy cienka warstwa krzemu porowatego — w zakresie od 550 do 750μm.

Przedstawiono model zmian strukturalnych w obszarach przypowierzchniowych płytki krzemowej wytworzonych w wyniku zastosowanych procesów technologicznych, jak również zaproponowano mechanizmy związane z pasmami elementarnymi w widmie fotoluminescencji.

1. Introduction

Porous silicon has become a very interesting material owing to its the room-temperature visible luminescence properties [1]. Porous silicon structures have been reported to luminesce efficientlly in the entire visible range, from the near infrared (~1500nm) to the near UV (~350nm) [2]. Still the origin of the efficient visible luminescence and electronic mechanisms involved in this effect are not clear. As the physical processes responsible for the light emission, the quantum confinement within silicon nanocrystals [1], emission from molecular species such as siloxene [3] and recombination near the Si/SiO_2 interface [4] or combination of these three mechanisms have been proposed.

The optical, electrical and physical properties of porous layer depend strongly on its microstructure. The mechanisms of the complex microstructural changes in near surface areas of silicon wafers occurring during porous layer formation are not yet fully understood. It is generally accepted that pore initiation occurs at surface active sites, defects or irregularities. The properties of porous silicon layer (porosity, thickness, pore diameter and microstructure) mainly depend on operating parameters of layer formation, including the HF/HNO_3 concentration ratio, the presence of surface active compound additives, the duration and the temperature of the process as well as the substrate doping types and the doping concentration. Thus the large variety of the porous structures can be produced.

Ion implantation has been extensively employed to modify the surface layers of materials and to synthesise new phases with novel properties. It is expected that for silicon substrate with such near-surface layer modification a new porous structure can be obtained.

The presented work is aimed at the investigation of structural changes in the modified n^+-type near-surface layer of silicon wafer, caused by ion implantation and/or a chemical etching as well as at their influence on the photoluminescence effect of thin porous silicon layers obtained in this way.

Therefore, in the presented work the structure of porous silicon layer was investigated using AFM and X-ray diffraction methods.

2. Experimental details

The substrate used in this work was p-type (111)-oriented monocrystalline Si wafer (diameter = 3in., thickness 250μm) with the n^+-p junction and BSF (Back Surface

Field). Both junctions (n^+-p and p-$p+$) were produced in one technological cycle as a result of the diffusion of phosphorous from $POCl_3$ source and the diffusion from Al paste.

To prepare the sample, a half of the Si wafer was implanted at room temperature with P^+ ions at dose $8 \times 10^{14}cm^{-2}$ and 180keV energy and than annealed for 30min at temperature 500°C. The final nanostructures were formed (only on a half of the implanted and non-implanted areas) by electroless chemical etching in solution containing concentrated HF, HNO_3, H_2O and same surface-active additives. Thus the sample contained four regions with different structural modification of the surface layers (as it is indicated in Fig. 1).

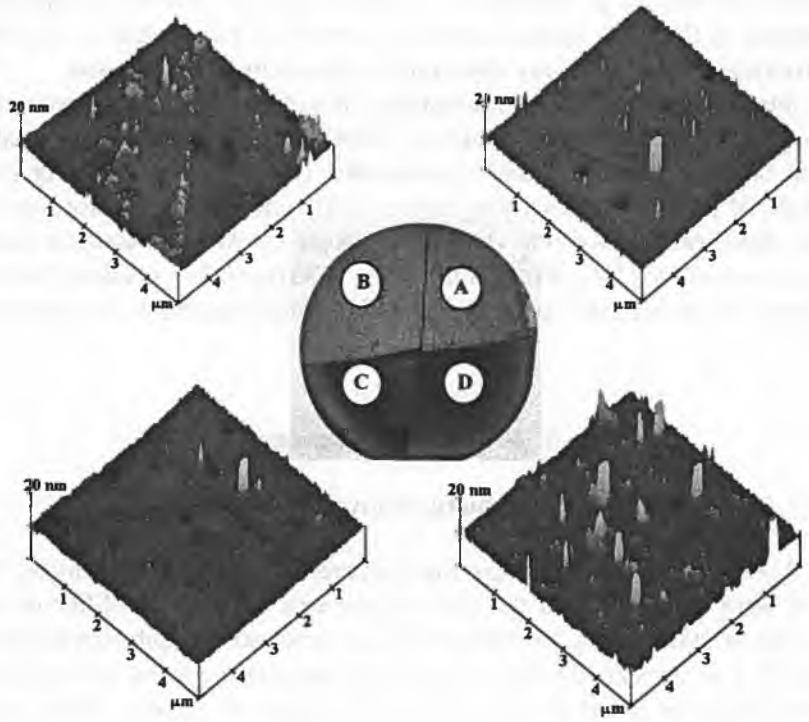

Fig. 1. General view of the silicon wafer and AFM images of surface morphology. The letters idicate regions obtained in the course of applied sample treatment. A — an initial material (n^+-type Si); B — anmplanted and annealed material; C — a thin porous silicon layer formed by chemical etching on the ion implanted and annealed n^+-type Si; D — a thin porous silicon layer formed by chemical etching on the n^+-type Si

Structural changes in the near-surface layers of sample caused by the ion implantation and/or chemical etching were analysed by means of the two-crystal diffractometry and the X- ray topography in the screw-asymmetrical mode of the Bragg diffraction. In the latter case the angles of the diffraction θ and disorientation Ψ (between entry

(111) and reflecting planes) insignificantly differ ($\theta - \Psi \approx -1°$). The angles of input and output of x-rays at the azimuth turn of crystal around diffraction vector at angle φ in skew- asymmetric scheme of the diffraction vary as follows [5]:

$$\sin(\phi_{0,h}) = \gamma_{0,h} = \pm \sin\theta \cos\psi - \cos\theta \sin\psi \cos\varphi. \quad (1)$$

The sign "+" concerns an incident ray and sign "-" diffracted one. From the Eq. (1) it follows, that at crystal turns on angle φ the smooth conversion from Laue diffraction to the Bragg diffraction is ensured. It should be noted, that contrary to usual geometry of diffraction, in skew-asymmetric scheme it is possible, by changing φ angle, to select cases, when layers studied have depths less then extinction length $L_{ex} = \frac{1}{|\chi_h|}\sqrt{\gamma_0|\gamma_h|}$, ($\chi_h$ - is Fourier coefficient of polarizability, λ - wavelength). In this way, X-ray topography measurements of thin near surface layers are possible. CuK_α radiation in a diffraction profile (rocking curve) and X-ray topography measurements were used.

The intensity distribution in near-surface layers of samples has been calculated on the basis of the numerical solution of Takagi-Taupin equations. The satisfactory agreement between theoretical and experimental rocking curves were derived using optimisation of parameters describing strain profile and structure distortions in depth.

X-ray structural investigation were accompanied by AFM measurements. Photoluminescence was excited by a nitrogen laser (λ_{ex} = 337nm). The resulting luminescence was dispersed by an infrared spectrometer IKS-12 and detected with a photomultiplier FEU-79.

3. Results and discussion

3.1. Structural investigations

Fig. 2 shows the series of X-ray topographies for investigated sample. The measurements were carried out in the skew-asymmetrical mode for different azimuthal angles φ and in other words, for different X-ray penetration depths (extinction lengths L_{ex}). The 331 $CuK\alpha_1$ reflection was used. The boundaries between four regions formed of different structural modification of the surface layers are clearly visible in X-ray topography. Depending on the input angle of X-ray beam, the differences arising between a reflectivity for each region are revealed. It may testify that the structural parameters of these regions differ significantly. It should be noted that stresses induced by the ion implantation and/or chemical etching processes are uniformly distributed within the bounds of respective regions. The degree of local structural disturbances of modified surface within the individual regions can be estimated also from AFM images (Fig. 1).

The quantitative picture of near-surface structural changes in described above regions was obtained from diffraction line profiles (rocking curves) for 111- and 333-$CuK\alpha_1$ reflections. From the performed analysis it appears that various treatments used in sample fabrication technology lead to different forms of rocking curves in relation to the rocking curve obtained for untreated part of the sample. Especially it concerns the

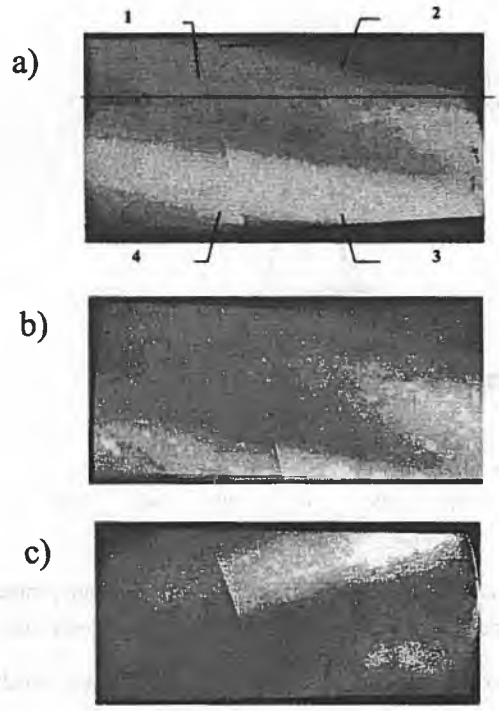

Fig. 2. The X-ray topographies measured in the skew-asymmetric mode for different input angles of X-ray beam Φ_0 (extinction length L_{ex}. A) $\Phi_0 = 7.5°$ ($L_{ex} = 1.5\mu m$); b) $\Phi_0 = 4°$ ($L_{ex} = 0.8\mu m$); c) $\Phi_0 = 1.5°$ ($L_{ex} = 0.3\mu m$

"tails" of the rocking curves. Moreover, it is observed that full width at half-maximum value (FWHM) of the rocking curves as well as the ratio of integral intensity to maximum insignificantly increase. From these observations it may be concluded that different structural disturbances in the near-surface layers of individual regions of the sample are present.

The intensity distributions in near-surface layers of sample have been calculated on the basis of the numerical solution of T a k a g i - T a u p i n equations. The satisfactory agreement between theoretical and experimental rocking curves were obtained using optimisation of parameters describing strain profile $\Delta d(z)/d$ and structure distortions $W(z)$ in depth.

Structural disturbance depth-profiles (strain and distortions) were chosen as a set of exponential peaks with different height, width and position of the maximum:

$$\frac{\Delta d(z)}{d} = \begin{cases} z_2 \cdot \exp\left[-\left(\frac{z-z_1}{2z_3}\right)^2\right], & \frac{\Delta d}{d} > z_5, i\ z \leqslant z_1 \\ z_5, & \frac{\Delta d}{d} \leqslant z_5\ i\ z \leqslant z_1 \\ z_2 \cdot \exp\left[-\left(\frac{z-z_1}{2z_4}\right)^2\right], & z > z_1 \end{cases} \quad (2)$$

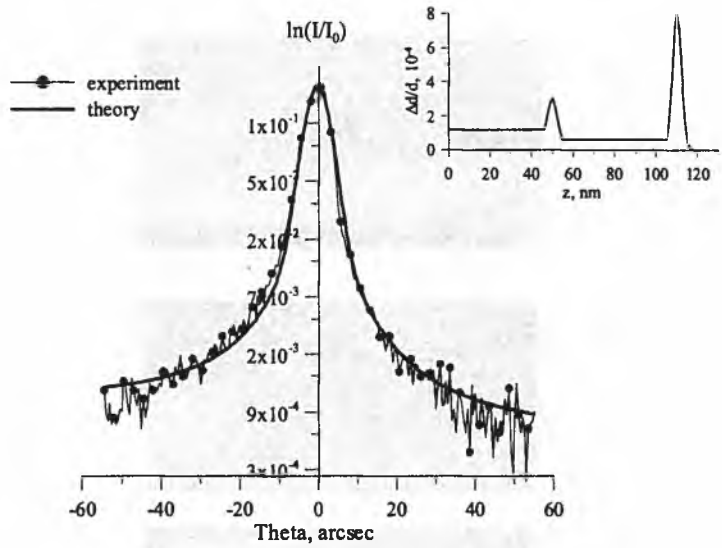

Fig. 3. The experimental and theoretical rocking curves and the strain profiles for an implanted and annealed material. The 333 CuKα reflection was used

For the optimisation of the parameters, the least square method was used to minimise the function:

$$F(z_1, z_2, ..., z_{10}, \Delta\theta) = \sum \rho_k \left[\frac{I_{\exp}(\Delta\theta_k) - I(z_1, z_2, ..., z_{10}, \Delta\theta_k)}{I_{\exp}(\Delta\theta_k)} \right]^2, \qquad (3)$$

where $I(z_1, z_2, \ldots, z_{10}, \Delta\theta_k)$ and $I_{exp}(\Delta\theta_k)$ are an intensity of the theoretical and experimental rocking curve in the point k, respectively; σ_k — weight function, $\Delta\theta_k = \theta_k - \theta_B$.

The strain profiles $\Delta d(z)/d$ obtained from computer simulation of rocking curves for each region of the sample are demonstrated in insets of Fig. 3 — 5. As it is shown in inset of Fig. 3, for the ion implanted and annealed region a strain profile $\Delta d(z)/d$ has two exponential peaks: the first peak with maximal value $\Delta d(z)/d\,|_{max} = 3 \times 10^{-4}$ at z_{max} = 50nm and the second one with $\Delta d(z)/d\,|_{max} = 8 \times 10^{-4}$ at z_{max} = 110nm. For the ion implanted and chemically etched region a strain profile $\Delta d(z)/d$ has one peak with the maximal value $\Delta d(z)/d\,|_{max} = 8 \times 10^{-4}$ at z_{max} = 90nm (see inset of Fig. 4), at the same time the constant deformation $\Delta d/d = 3 \times 10^{-4}$ reaching a depth of 85nm is present. The characteristic feature of the chemically etched region (inset of Fig. 5) is presence of the constant deformation $\Delta d/d = 7 \times 10^{-4}$ up to a depth of 50nm and a exponential profile of strain with the maximum $\Delta d(z)/d\,|_{max} = 5 \times 10^{-4}$ at z_{max} = 120nm.

As it follows from AFM measurements (Fig. 1), the minimal diameter of quantum wire and a size of cluster are a few nanometers.

The largest mean roughness R_a = 0.398nm is characteristic for the chemically etched region of the sample. For the ion implanted region and the ion implanted and

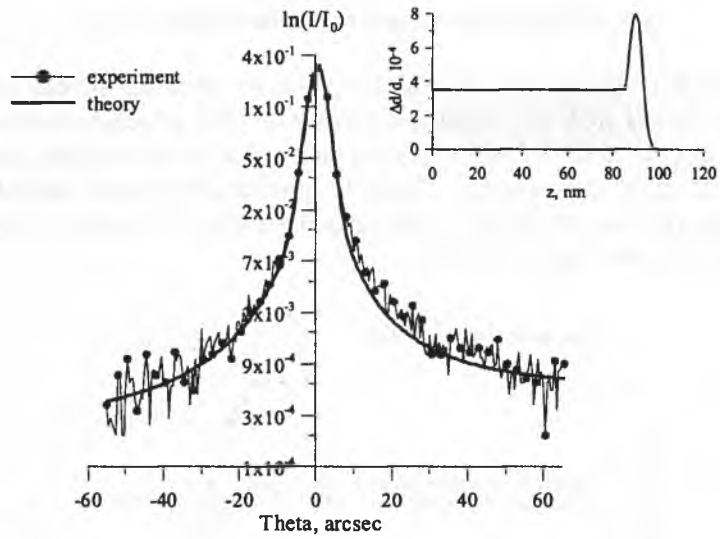

Fig. 4. The experimental and theoretical rocking curves and the strain profiles for a thin porous silicon layer formed by chemical etching on the ion implanted and annealed n^+-type Si. The 333 CuKα reflection was used

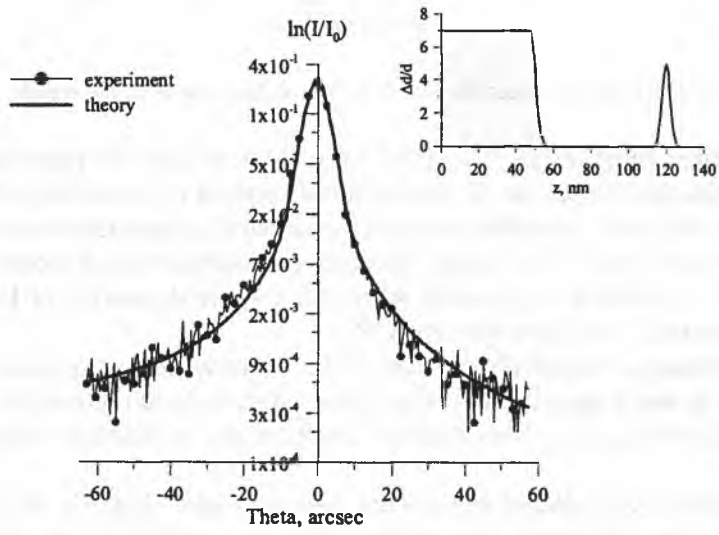

Fig. 5. The experimental and theoretical rocking curves and the strain profiles for a thin porous silicon layer formed by chemical etching on the n^+-type Si. The 333 CuKα reflection was used

chemically etched region R_a equals 0.288 nm and 0.303nm, respectively. The initial material is characterised by the least value of mean roughness R_a = 0.17nm.

3.2. Photoluminescence of porous silicon layer

Fig. 6 shows photoluminescence spectra obtained from the porous silicon layers formed on an initial and ion implanted substrates. The photoluminescence spectra derived from porous area at long-term exposure and after of exciting luminous flux, revealed the effect of luminescence "fatigue" (photoluminescence degradation under normal photoexcitation conditions) and spectral shift to red region. Explanation of these effects can be find in [6] and [7].

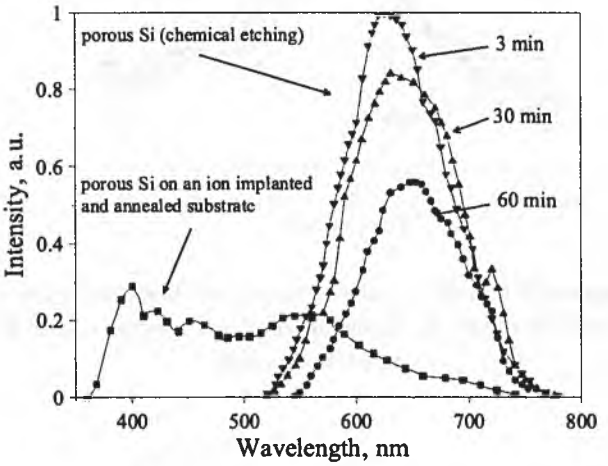

Fig. 6. Photoluminescence spectra (PL) from different areas of the sample

Many various mechanisms have been proposed to explain the photoluminescence properties of porous silicon, but the quantum confinement model seems to be the most useful. Porous silicon is generally described as a mixture of quantum wires of different concentrations and sizes. In a simple quantum confinement-based model the visible luminescence is produced in quantum wires and a spectral position of luminescence bands are associated with their diameters [7].

Non-homogeneous depth-distribution of the diameter size of quantum wires has been reported in many papers concerning porous silicon nanostructures. In the case of thin porous silicon layers a "two-humped" depth-profile of diameter sizes should be expected.

As it follows from photoluminescence measurements (Fig. 6), the increase of exposure time leads no simply to a photoluminescence redshift but to a relative drop of photoluminescence intensity of the first band and at the same time to relative increase of photoluminescence intensity of the second band. In this way the spectral shift occurs as a redistribution of photoluminescence intensity between two bands.

The presence of two different components in a luminescence spectra has simple interpretation. According to [6], two components in a luminescence spectra correspond to two groups of quantum wires in the diameter distribution. In this way, the obtained

results display a relation between the energy (wavelength) of recombination radiation and a structural feature of porous silicon.

At the stage of continuous illumination of the sample, the photoluminescence intensity decreases due to the luminescence fatigue effect. The luminescence fatigue effect can be explained as a result of nonradiative centres photoactivation.

The excitation of carriers and their radiative recombination depend strongly on structural factors of porous silicon layer. Adsorbes molecules as well as surface defects generate different types of radiative and nonradiative centres on Si-wire surface. According to [7], the probability of nonradiative recombination W_{nr} is proportional to the number of nonradiative centres N_{nr} in volume where carrier drift takes place:

$$w_{nr} \sim N_{nr} \tag{4}$$

The number of nonradiative centres N_{nr} can be simple expressed by their concentration N_{nr}(t) (which is a time function as a result of fatigue effect), the carrier drift velocity V and the time of carrier drift T_d:

$$N_{nr} = n_{nr}(t)SVT_d. \tag{5}$$

Prolongation of a set value of T_d during experiment leads to registration of these luminescence components for which significant increase in w_{nr} takes place, what manifests as faster intensity relaxation of slow components on the experimental curves (Fig. 6).

The observed spectral features of fatigue effect results also from Eq. (5). Electron-hole pairs are generated by photons with energy E_0 whereas the photoluminescence spectra spreads over a wide energy range. The energy of the emitted photons E_{lum} during electron-hole recombination depends on the energetic position of quantum state participated in the radiative recombination process. Then, the longer wavelength of luminescence ($\lambda_{lum} = hc/E_{lum}$) the highest loss of electron-hole pairs energy ($\Delta E = E_0 - E_{lum}$) before the radiative recombination process.

According to [8], the mean carrier-drift velocity V is proportional to the square root of energy losses during the carrier drift:

$$V \sim (E_0 - E_{lum})^{1/2} \tag{6}$$

Then the probability of nonradiative recombination has the maximal value for electron-hole pairs, which recombine with large delay on the long-wave spectrum range.

A combination of Eq. (5) and dependence (6) leads to the expression for a decrease of luminescence intensity arising from the fatigue effect:

$$[I(0) - I(t)] \sim n_{nr}(t)ST_d(E_0 - E_{lum})^{1/2}. \tag{7}$$

From relation (7) it follows that the luminescence fatigue results from time evolution of nonradiative centres concentration n_{nr}. Kinetic behaviour of this phenomenon is

manifested in an asymmetrical broadening of luminescence band. The same concentrations of nonradiative centres lead to different probability of nonradiative recombination for different components of the band. For given increase of nonradiative centres concentration n_{nr}, the right-hand side of relation (7) quickly increases for the "slow" (with a long time T_d) and long-wave (with a big energy difference E_0–E_{lum}) components.

The drop of photoluminescence intensity of the fundamental band and appearance of greater amount of additional bands in a short-wave range of luminescence spectra, obtained for porous silicon prepared by the ion implantation followed by chemical etching, can be explained by an influence of intrinsic electric field generated by charged donors and post- implanted defects. It manifests itself in a decrease of probability of radiative recombination (in the spectral range of fundamental band) and in creation of additional channels for the radiative and nonradiative recombination which interaction generates "white" luminescence. Additional possible reason for observed blue-shift of photoluminescence is a change of quantum confinement effect by the formation of small nanocrystals. These small nanocrystals might have been formed under the surface damage layer by chemical etching.

4. Conclusions

In the present study, the effect of phosphorous ion pre-implantation on photoluminescence spectrum of porous silicon layer was investigated. The porous silicon layer produced by only chemical etching exhibits a room temperature photoluminescence at ~550-750nm. The photoluminescence spectrum derived from porous area at long-term exposure and action of exciting luminous flux revealed the effect of luminescence "fatigue" and spectral red-shift. The luminescence fatigue effect can be explained as a result of nonradiative centres photoactivation, where as the spectral shift as a redistribution of photoluminescence intensity between two elementary bands arising from two groups of quantum wires in the diameter distribution.

In addition to the weakening and shift of main spectral band to red region, the appearance of extra bands in the short-wave region of spectrum were observed on the photoluminescence spectrum for porous layer prepared by an ion implantation followed by annealing and chemical etching. This is due to the structural change of porous silicon layer formed on the n^+-type Si with near-surface damaged thin layer.

REFERENCES

[1] L.T. Canham, Appl. Phys. Lett. **57**, 1046 (1990).
[2] A.G. Cullis, L.T. Canham, P.D.J. Calcott, J. Appl. Phys. **82**, 909 (1997).
[3] Z.Y. Xu, M. Gal, M. Gross, Appl. Phys. Lett. —bf60, 1375 (1992).
[4] S.M. Prokes, Appl. Phys. Lett. **62**, 3244 (1993).

[5] A.M. Afanas'ev, P.A. Aleksandrov, R.M. Imamov, X-ray diffraction of submicron layers, Nauka, Moska, 1989.
[6] S.P. Zimin, Fizika i Tekhnika Poluprovodnikov **34**, 359 (2000) (in Russian).
[7] M.E. Komnan, V.E. Harciev, I.Y. Shabanov, Fizika Tvierdovo Tiela **39**, 2137 (1997) (in Russian).
[8] M.E. Komnan, I.Y. Shabanov, Fizika Tvierdovo Tiela **39**, 1165 (1997) (in Russian).

Received: 21 March 2005.